Ab Initio Study of the Structure of the α-MoO_3 Solid and Study of the Adsorption of H_2O and CO Molecules on Its (100) Surface

Aristotle Papakondylis[†] and Philippe Sautet*

Laboratoire de Chimie Théorique, Ecole Normale Supérieure de Lyon 46, Allée d'Italie, 69364 Lyon Cedex 07, France, and Institut de Recherche sur la Catalyse, 2, avenue A. Einstein, 69626 Villeurbanne Cedex, France

Received: December 13, 1995[⊗]

Ab initio periodic Hartree−Fock calculations along with corrections for correlation effects have been carried out to study the crystal structure of α-MoO_3. The nature and energetics of bonding within the solid have been investigated and related to the geometry of the crystal. $(MoO_3)_x$ chains formed by MoO_4 tetrahedra sharing common O corners were shown to be the basic structural units of the solid. Simple Mo···O electrostatic interactions between these chains lead to the formation of the natural layers of MoO_3 and establish a 6-fold coordination around Mo atoms. The (100) surface of α-MoO_3 solid contains pentacoordinated Mo atoms, brought about by the breaking of interchain interactions, and possessing a Lewis acid character. The adsorption of H_2O and CO molecules on these Mo sites was found to be of, essentially, electrostatic nature restoring a bulklike environment around Mo atoms.

1. Introduction

Molybdenum oxides, like other group 6A element oxides, are known to present an important stoichiometric and structural variety.[1] However, only two of them are stable above 1000 °C, namely MoO_3 (Mo^{VI}, oxide α) and MoO_2 (Mo^{IV}, oxide δ). Successive reduction of MoO_3 gives raise to intermediate mixed valence compounds such as Mo_4O_{11}, Mo_5O_{14}, Mo_8O_{23}, and Mo_9O_{26}. These structures are made up by corner- and/or edge-sharing MoO_6 distorted octahedra and/or MoO_4 tetrahedra, and their crystal structures were proved[2−6] to be shear structures consisting of largely unchanged slabs of a base structure.

The physicochemical properties of molybdenum oxides are widely exploited in heterogeneous catalysis. Lattice oxygen mobility, existence of Lewis acid-base sites, and selectivity as a function of the different exposed faces are some of their properties finding important applications in the field of mild oxidation reactions.[7] α-MoO_3, often supported or mixed with other metal oxides, has been shown to be a performant catalyst in the oxidation reactions of olefins[7−10] and alcohols.[11−13] However, the elementary steps of catalytic processes and the specific role of each crystal face are objects of some controversy between researchers. For instance, in the case of propene oxidation to acrolein, Volta et al.[7−9] claimed that the reaction takes place on the (100) face while Brückman et al.[10] concluded that basal face (010) is more favorable to this process.

Empirical models have been presented[14] in order to rationalize catalytic reaction mechanisms, and much experimental work has been carried out to this end. Lewis acid centers on the (100) surface are considered to be important for olefin adsorption and intermediate species stabilization[15] while Mo═O or O−Mo−O oxidizing centers are responsible for the oxygen insertion step as it was shown by studies using ^{18}O isotopic labeling. Oxygen diffusion from bulk to reoxidize surface Mo centers has been found to be important.[17] Raman spectroscopy studies[18] indicated that lattice deficiencies of the type MoO_{3-x} should play a role in the oxygen exchange and catalytic properties of α-MoO_3.

A study of the electronic and geometrical structure of the solid[19] by XPS and LEED techniques revealed that the valence band width of MoO_3 is 7 eV and that its crystal structure consists of an integral number of intact double layers parallel to the (010) face. Surface (010) geometry was shown to be identical with the bulk geometry as no bond must be broken to form it (natural cleavage).

Although a large experimental literature exists on MoO_3, and we do not attempt to exhaust it here, little theoretical work was found for this system, mainly semiempirical calculations on cluster models. SCF-SW-X_α calculations were performed by Broclawik et al.[20] on simple and double octahedral models aiming to interpret the innershell photoelectron spectra of MoO_3. Periodic extended Hückel calculations by Sylvestre[21] explained how prereduction of the (100) surface could affect the catalytic properties of MoO_3. However, we remark that in the above studies idealized perfect octahedral geometries were used with Mo−O bond lengths differing significantly from the experimental values.[4] Semiempirical ASED-MO calculations on cluster models have been reported by Anderson et al.[22] and Kang et al.[23] examining the elementary steps of olefin oxidation. A series of papers by Rappé and Goddard III[24] presented *ab initio* GVB + CI results on molecular models (e.g. Cl_2MoO_2), suggesting the importance of spectator oxo Mo═O groups in the catalysis of hydrocarbon oxidation and olefin metathesis reactions. Rahmouni et al.[25] presented a study of the interaction of methanol with MoO_3 finite clusters using extended Hückel methodology.

In the present paper we present, for the first time, *ab initio* Hartree−Fock periodic calculations on α-MoO_3 solid. A stepwise reconstruction of the system is carried out; going from molecular MoO_3 to the three-dimensional system, we investigate the electronic structure and the nature of the bonding within the solid.

Finally, we use an infinite model of the (100) surface to study the interaction of small molecules, H_2O and CO, with Lewis acid Mo centers present on this surface.

2. Methodology and Computational Details

We performed periodic Hartree−Fock calculations on the infinite 1D, 2D, and 3D systems implied in our study (*vide*

* Corresponding author; e-mail: sautet@chimie.ens-lyon.fr.
[†] Present address: Laboratory of Physical Chemistry, Department of Chemistry, University of Athens, Panepistimiopolis, Athens 15771, Greece.
[⊗] Abstract published in *Advance ACS Abstracts,* May 15, 1996.

S0022-3654(95)03727-0 CCC: $12.00 © 1996 American Chemical Society

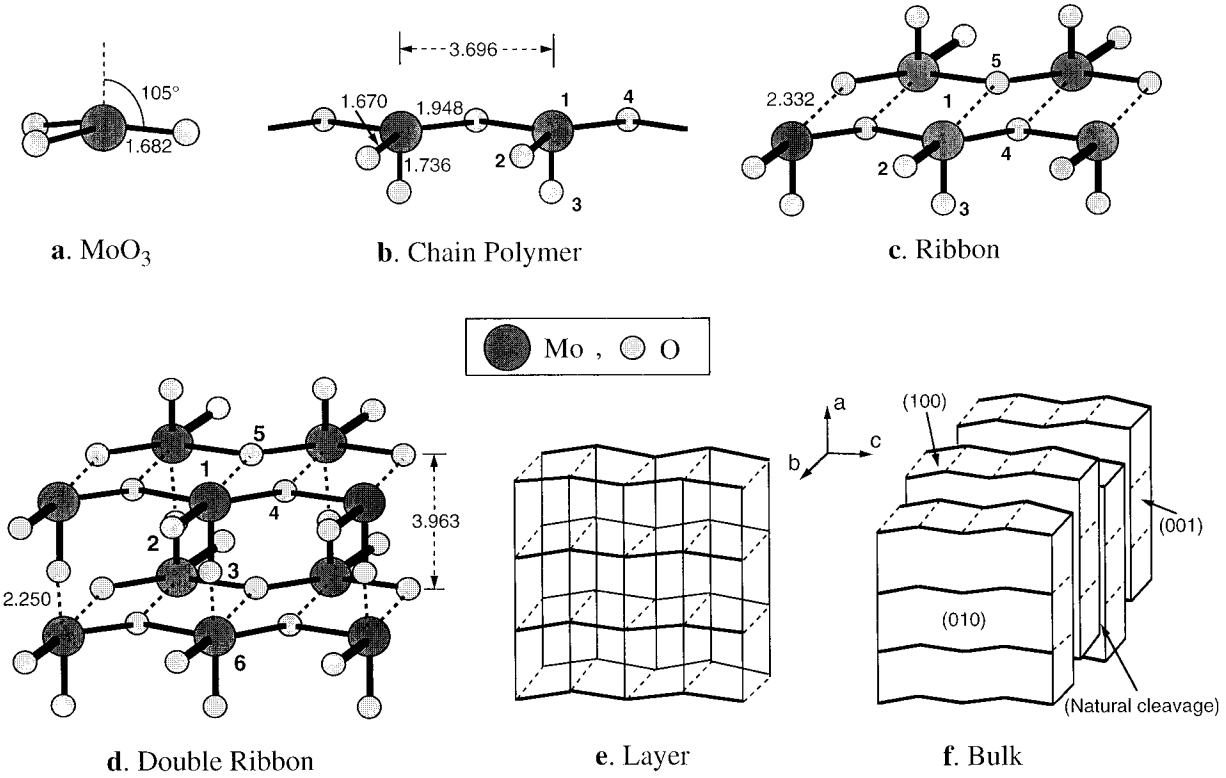

a. MoO_3 **b**. Chain Polymer **c**. Ribbon

d. Double Ribbon **e**. Layer **f**. Bulk

Figure 1. One-, two-, and three-dimensional models used in the study the α-MoO_3 crystal structure. Distances are given in angstroms.

infra). The Hartree−Fock (H−F) energy values have been corrected for correlation by density functional type calculations[27−29] integrating the H−F SCF electron density; two different functionals are employed, namely those of Colle−Salvetti[29] and the Perdew 91.[27]

The inner core electrons of Mo, O, and C atoms were replaced by effective core potentials (ECP). For Mo we used the Hay and Wadt[30] small-core potential retaining 14 valence electrons in our calculations while the $1s^2$ electrons of O and C were replaced by Barthelat's[31] ECPs. The basis set used to describe the valence space of a molybdenum atom consists of (5s6p4d) gaussian type functions contracted to [3s3p2d].[30] For the O and C atoms we used[32] (5sp) gaussian basis sets contracted to [2s2p] as follows:

oxygen			carbon		
exp	C_s	C_p	exp	C_s	C_p
23.711 724	0.016 944	0.026 384	9.883 991	0.017 722	0.029 235
6.226 854	−0.161 506	0.115 073	3.094 801	−0.172 299	0.109 637
2.108 452	0.112 376	0.298 993	0.900 475	0.234 822	0.379 339
0.706 472	0.669 954	0.470 880	0.275 365	0.697 045	0.490 890
0.221 265	1.0	1.0	0.102 028	1.0	1.0

These bases were completed by a d polarization function with exponent 0.6 for both O and C atoms. Finally, for hydrogen atoms we used a standard (4s) contracted to [3s] basis set.

The geometrical parameters of the solid used through this work were set to the experimental X-ray values reported by Kihlborg.[4] In some cases we give results of partial optimizations and molecular type calculations, for the sake of comparison. Adsorption geometries were manually optimized keeping the surface geometry frozen. The space symmetry was exploited in all cases and a cutoff of 10^{-5} was used for integrals.

All computations were done using the CRYSTAL95 program[33] on IBM/RS6000 workstations. For some molecular calculations the GAUSSIAN94 system[34] was employed.

3. The α-MoO_3 Solid

MoO_3 crystallizes in the space group *Pbnm*-D_{2h}[16] (No. 62 of Intl. Tables in an alternative orientation) with four MoO_3 units in the unit cell. The orthorhombic unit cell is of the following dimensions: $a = 3.963$ Å, $b = 13.855$ Å, and $c = 3.696$ Å. The solid is characterized by a layered structure with a van der Waals inter-layer distance of ∼6 Å. The geometrical structure of MoO_3 as established by Kihlborg's[4] accurate X-ray analysis, shows that molybdenum atoms are surrounded by four close neighbor oxygen atoms at distances 1.94, 1.95, 1.73, and 1.67 Å and two oxygen atoms at significantly longer distances: 2.25 and 2.33 Å. These values clearly indicate that, from a geometrical point of view, three different types of oxygen neighbors are present in the coordination sphere of molybdenum atoms. In earlier studies the MoO_3 structure was considered to consist of MoO_6-distorted octahedra connected by common edges in the *c*-axis direction. However, Kihlborg's analysis showed that the four close oxygen neighbors tend to have a rather tetrahedral arrangement around Mo atoms, with O−Mo−O angles (143°, 104°, and 98°) differing significantly from the octahedral 180° and 90° values. α-MoO_3 can, therefore, be thought of as built up by MoO_4 tetrahedra sharing common oxygen corners and forming chains in the direction of the *c*-axis, with additional interactions between those chains building 2D layers.

In this work we followed Kihlborg's view for MoO_3 construction; we started from the MoO_3 molecule (Figure 1a), and then we studied its polymeric chain form (Figure 1b) which was used as a structural unit to build (100) ribbons (Figure 1c), (010) layers (Figure 1e), and finally MoO_3 bulk (Figure 1f). The nature of the Mo−O interactions brought about was analyzed in order to provide a "chemical-bonding" interpretation of the O coordination around Mo atoms.

The main results of our study are reported in Table 1 while DOS (density of states) curves are presented in Figure 2.

3.I. Molecular MoO_3. The MoO_3 molecule is of C_{3v} symmetry (Figure 1a) with three equivalent Mo═O bonds. Each O(^{3}P) atom forms a double (one σ and one π) bond employing two electrons of the central Mo(^{7}S) atom. Molybdenum atom can be thought to be in a formal Mo^{VI} oxidation state. Our H−F SCF calculations yielded a Mo−O bond length of 1.682

TABLE 1: Absolute Energies E (E_h), Binding Energies BE (kcal·mol^{-1}), Fermi Levels E_f (E_h), Mulliken Net Charges q, and Overlap Populations S for the Different MoO_3 Models[a]

	MoO_3	chain polymer	ribbon	double ribbon	layer	bulk
E_{SCF}	−113.97571	−114.06122	−228.16410[c]	−456.35492[d]	−228.21915[c]	−456.43448[d]
BE (SCF)[b]	−53.7	0.0	13.1	17.3	30.4	29.8
E_f	−0.47204	−0.46400	−0.51020	−0.48970	−0.51480	
$E_{SCF+Correl}$[e]	−115.08223	−115.17540	−230.41297	−460.88240	−230.49793	−461.01672
BE (SCF + Correl)[b]	−58.5	0.0	19.5	28.4	46.2	49.4
$E_{SCF+Correl}$[f]	−115.27967	−115.36917	−230.80241	−461.65927	−230.88561	−461.78415
BE (SCF + Correl)[b]	−56.2	0.0	20.1	28.6	46.2	48.2
q[Mo(1)][g]	+2.64	+2.76	+2.85	+2.98	+3.04	+3.07
q[O(2)][g]	−0.88	−0.73	−0.77	−0.73	−0.75	−0.79
q[O(3)][g]	−0.88	−0.78	−0.75	−0.96	−1.02	−1.02
q[O(4)][g]	−0.88	−1.25	−1.33	−1.30	−1.27	−1.26
S[Mo(1)−O(2)][g]	0.19	0.25	0.23	0.25	0.23	0.17
S[Mo(1)−O(3)][g]	0.19	0.30	0.29	0.17	0.05	0.05
S[Mo(1)−O(4)][g]	0.19	0.11	0.05	0.07	0.07	0.06
S[Mo(1)−O(5)][g]			0.05	0.07	0.05	0.05
S[Mo(6)−O(3)][g]				0.07	0.07	0.07

[a] See Figure 1. [b] Binding energy per MoO_3 unit with respect to the polymer model. [c] Unit cell containing $2MoO_3$. [d] Unit cell containing $4MoO_3$. [e] SCF + correlation correction energy using the Colle−Salvetti[29] density functional. [e] SCF + correlation correction energy using the Perdew 91[27] density functional. [f] For atom numbering, see Figure 1.

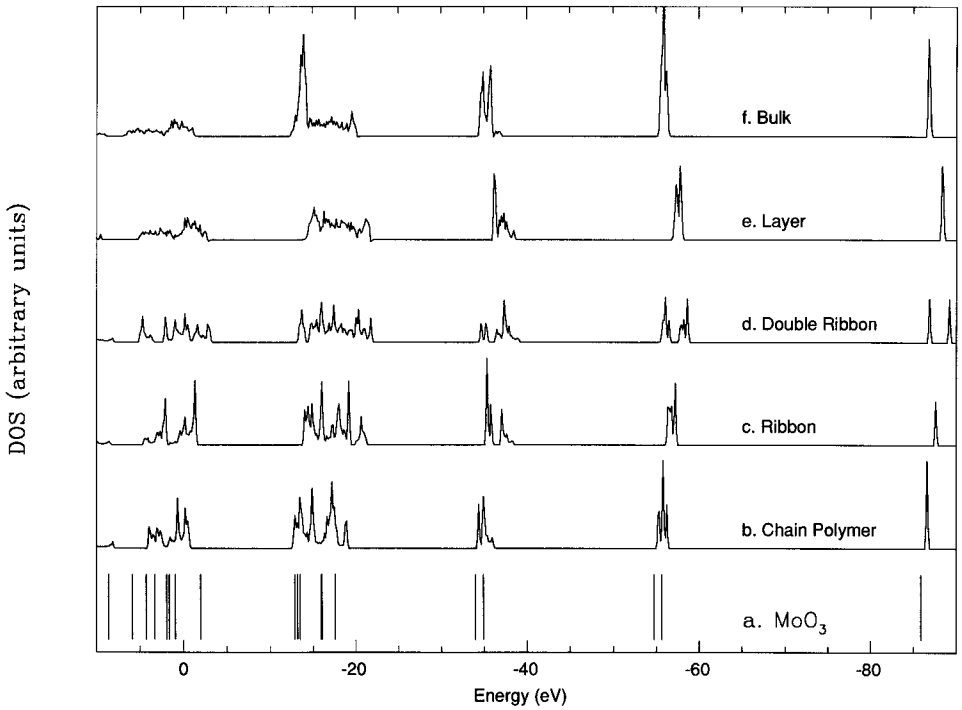

Figure 2. Molecular orbital levels of MoO_3 molecule (a) and total density of states (DOS) curves of the different models (b−f) presented in Figure 1.

Å and showed that the molecule is nonplanar, the Mo−O bonds forming an angle of 105° with the C_3 axis. Using correlation corrections, we obtained the values 1.766 Å and 112°, respectively, for these parameters. The Mo−O bond length values obtained are very similar with the 1.670 and 1.736 Å values encountered in α-MoO_3 crystal. The bent geometry of the molecule can be explained considering the attractive interactions arising between p orbitals of O atoms and the $4d_{z^2}$ orbital of Mo (considering z-axis ≡ C_3 axis).

In Figure 2a, we have reported MO levels obtained through H−F SCF calculations. At −86 and −55 eV we have the 4s and 4p levels of Mo, respectively, while at −35 eV the oxygen's 2s levels are present. In the region −13/−18 eV there are Mo−O bonding MOs, mainly oxygen 2p with a minor Mo 4d/5s contribution, and nonbonding (lone-pair) O levels. The levels observed around 0 eV are virtual orbitals, Mo−O antibonding, with a predominant Mo 4d/5s character.

From Table 1, we can see that Mo−O bonds bear a marked ionic character. Mulliken population analysis yields a net charge −0.88 on oxygen atoms and the Mo−O overlap population, 0.19, is rather small for a typical covalent double bond.

Concerning the Mo−O bond energy, we would like to remark here that H−F SCF calculations failed dramatically to predict a good atomization energy value for the MoO_3 molecule; we calculated an endothermicity of 63.5 kcal·mol^{-1} for the reaction $MoO_3(^1A_1) \rightarrow Mo(^7S) + 3O(^3P)$, which is too small compared with the experimental[35] value 411 ± 7 kcal·mol^{-1}. Using the density functional type corrections for correlation, we obtained a value of ∼312 kcal·mol^{-1}, while at the MP2 level of theory the computed number was 444 kcal·mol^{-1}. Undoubtedly, high-quality correlation calculations are necessary to deal with energies of processes involving Mo−O bond breaking.

3.II. The Chain Polymer. Our next step was to consider the infinite chain polymer model of MoO_3, shown in Figure 1b. As it can be seen, it comprises MoO_4 tetrahedra linked by common O corners. It is noteworthy, here, that fragments of this type of chain, of the general formula $(MoO_3)_x$, in the form of puckered rings, were found to be the major components of

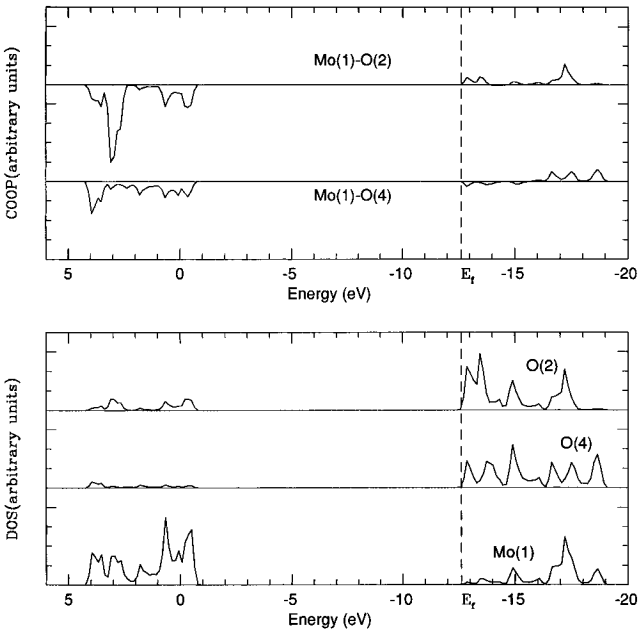

Figure 3. Bottom: Projected DOS curves on Mo(1), O(2), and O(4) atoms of the chain polymer model of MoO_3. Top: Crystal orbital overlap population (COOP) curves for the Mo(1)−O(2) and Mo(1)−O(4) bonds in the same model.

MoO_3 vapors obtained after sublimation of MoO_3 solid.[36] Also, molybdate species $[MoO_4]^{2-}$, $[Mo_2O_8]^{2-}$ in solution exhibit similar geometries.[1]

We can imagine as a first step for polymerization the decoupling of a bonding electron pair in MoO_3 molecule to form a $O_2Mo^{\bullet}-O^{\bullet}$ species which, in turn, polymerizes to give chain products. According to our H−F SCF theoretical results (Table 1), the overall process is exothermic by 53 kcal·mol^{-1} of polymerized MoO_3 (56−58 kcal·mol^{-1}, including correlation corrections). Certainly, these numbers are to be taken with some precaution because of the methodological pitfalls discussed before, and because of the unoptimized geometry used for the MoO_3 chain. However, *ab initio* molecular calculations for the cyclic dimer Mo_2O_6 yielded similar values for exothermicity (SCF, 48; MP2, 50 kcal mol^{-1}), and optimized bond lengths were close to the ones employed here: Mo═O, 1.680 (SCF) and 1.760 Å (MP2); Mo−O, 1.944 (SCF) and 1.946 Å (MP2).

Figure 2b displays the DOS curve obtained by periodic Hartree−Fock calculations. We observe that it, essentially, fits the level distribution of molecular MoO_3. The valence band is spread out over a range of 6.8 eV which is in good agreement with the experimental[19] bandwidth value of 7 eV. As we can see from Figure 3, the top of the valence band consists mainly of nonbonding levels, hosting oxygen lone electron pairs, and some Mo(1)−O(2) bonding contributions, while the middle and lower parts contain bonding Mo(1)−O(2,3) and Mo(1)−O(4) levels. Note that the participation of Mo orbitals in Mo(1)−O(2,3) bonds is more pronounced than in the Mo(1)−O(4) bonding levels.

The Fermi level is located at −12.6 eV (the zero of potential being defined at an infinite distance from the chain). The empty band between −1 and 4 eV is of a marked Mo 4d/5s character and contains antibonding Mo−O combinations. The system, evidently, is not a conductor, but the gap between the valence band and the first empty band, shown in Figure 3, must not be considered as the corresponding real bandgap because, as we know, the virtual SCF levels are, generally, no good for the description of excited states.

From Table 1, we see that the electron density distribution within MoO_3 units has been affected by polymerization. First, we observe that the two double bonds, Mo(1)−O(2,3) become less ionic with smaller net (negative) charges on O atoms and increased overlap populations. Second, the Mo(1)−O(4) simple bonds linking adjacent MoO_4 tetrahedra increase their ionicity, leading to a net charge of −1.25 on oxygen atoms. It seems that the two σ interactions of O(4) with two neighbor Mo atoms result in an easier electron transfer. The net result is a more pronounced cationic character for Mo atoms. The important stabilization of MoO_3 entities may be attributed (i) to the replacement of a Mo═O bond by two σ (Mo−O−Mo) bonds and (ii) to a further stabilization of the remaining two Mo═O bonds, which is similar to the spectator oxo group effect, described by Rappé and Goddard.[24]

3.III. The Ribbon Model. This model is constructed by putting together two chain polymers as shown in Figure 1c. Each molybdenum atom of the first chain is placed opposite to a linking O(4) atom of the second chain. We have adopted here the same atom arrangement as in MoO_3 crystals. The unit cell contains two MoO_3 formula units related to each other by a rotoreflexion element of symmetry. The interchain distance used in our calculations was 2.332 Å, a value which practically coincides with the H−F SCF optimized value of 2.330 Å.

According to our H−F SCF results, this chain polymer coupling leads to an energy gain of 13.1 kcal·mol^{-1} (∼20 kcal·mol^{-1} with correlation corrections) for each MoO_3 unit, with respect to the energy value of the chain polymer.

We turn now to the electronic structure of the ribbon model, trying to get some insight into the nature of the stabilization. From Figure 2c, we can see that all levels are uniformly downshifted. Moreover, the valence band becomes wider (∼7.6 eV), mainly because of a further lowering of p orbitals of O(4) atoms occupying the undermost part of the band. The nature of the interchain Mo(1)−O(5) interactions, responsible for these effects, is of a particular interest since one could expect that Mo atoms should act like Lewis acids, attracting electron density from oxygen atoms to form dative bonds. However, from Table 1 we see that such a hypothesis may not be justified, since the negative charge on O(4,5) atoms increases and so does the positive charge on Mo atoms. The overlap population for Mo(1)−O(5) is close to zero, and the same stands for the Mo(1)−O(4) intrachain bonds. The latter gets an entirely ionic character, clearly induced by the second chain.

Concerning the Mo═O double bonds, they remain practically unchanged as they were kept away from any interaction.

In conclusion, our analysis reveals that interchain interactions are of preponderant electrostatic character while intrachain ionicity increases due to mutual interchain electrostatic induction. This situation is illustrated by the electron density map of Figure 4A, showing the electronic distribution over the ribbon structure.

3.IV. Double Ribbon and Layer Models. From experimental X-ray analysis, we know that the natural layers present in the MoO_3 crystals are built up by ribbons as those presented in the previous section, running in the direction of the *c*-axis and piled up in the *a*-axis direction, as shown in Figure 1d,e. We note here that crystals of MoO_3 usually grow in the form of needles or platelets in the direction of the *c*-axis, just like ribbons.

In a first stage toward layer construction, we studied the case of a double ribbon system (Figure 1d). This system will be used later as a model of the (100) surface of MoO_3. As we can see, the interribbon interactions take place between molybdenum atoms and one of the "double-bonded" oxygen atoms. For the distance of 3.963 Å between ribbons, the Mo(6)−O(3) (Figure 1d) distance is 2.250 Å. Our results (Table 1) at the H−F SCF level of theory revealed an attractive interaction of

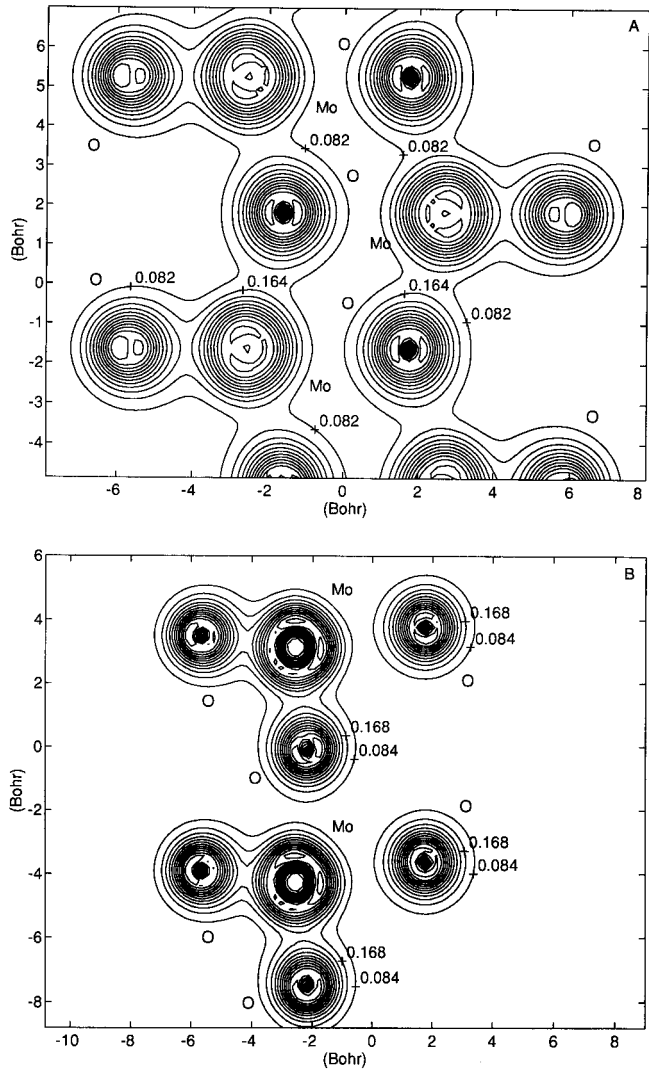

Figure 4. (A) Total electronic charge density map for the ribbon model, through a plane containing O(4) type atoms of the two parallel chains. (B) Total electronic charge density map for the double ribbon model, through a plane containing Mo(1), O(2), and O(3) atoms (see Figure 1 for atom numbering). All values of isodensity lines are given in e/bohr^3.

8.4 kcal mol^{-1} (∼17 kcal·mol^{-1}, including correlation corrections) for each interribbon interacting pair of MoO_3 units. Optimization of the interribbon separation at the H−F SCF level gave value of 4.222 Å, that is, a relaxation of 0.26 Å with respect to the experimental value for the crystal, which modifies the aforementioned interaction energy to 11 kcal·mol^{-1}

The corresponding DOS curve of Figure 2d exhibits a splitting of the 4s and 4p levels of molybdenum atoms, reflecting the existence of two different types of Mo, namely one with 5-fold and another with 6-fold oxygen coordination (in contrast with the ribbon model containing only 5-fold coordinated Mo atoms). This is an important feature of the (100) surface of the solid where the presence of pentacoordinated Mo atoms is responsible for the adsorption of various molecules. The valence band has spread out, reaching a width of 8.6 eV, while the Fermi level has not been modified significantly.

From population analysis, Table 1, we can infer that the interribbon bonding mode is, essentially, the same as in interchain bonding; Mo(1)−O(3) bonds increase their ionicity and new O(3)···Mo(6) electrostatic interactions occur. The electron density map presented in Figure 4B indicates the similarity between O(3)···Mo(6) and Mo(1)···O(5) interactions.

We consider now the infinite 2D layer as presented schematically in Figure 1e. This is one of the layers constituting α-MoO_3 crystals with its (010) face representing the natural cleavage basal planes of the solid (see Figure 1f).

Table 1 shows that the formation of the layer results in an energy gain of 17.3 kcal·mol^{-1} at the H−F SCF level (∼26 kcal·mol^{-1} with correlation corrections) per MoO_3 unit, with respect to the noninteracting ribbon systems. This value, representing two interribbon interactions for each MoO_3, is greater than double the corresponding value in the double ribbon model. An explanation to this may be the enhanced ionicity of Mo(1)−O(3) bonds, rendering electrostatic interactions stronger.

The optimization of the interribbon distance (cell parameter *a*) yielded a value of 3.920 Å which is close to the experimental value, 3.963 Å. We remark the difference with the corresponding distance in the double ribbon model, showing the importance of packing forces (long-range electrostatic interactions) in the layer.

From Figure 2e, we see that there are no more splitted Mo 4s and 4p levels, as all molybdenum atoms have now an identical environment (6-fold coordination) and that the valence band has become narrower (7.8 eV) with a Fermi level at −14 eV.

3.V. The Bulk. The final step was to form α-MoO_3 bulk by superposing layers in the *b*-axis direction, as shown schematically in Figure 1f. Each layer is displaced by *a*/2 in the *a*-axis direction, relative to the next layer. The unit cell contains four MoO_3 units and extends over one layer and two half layers above and below the latter. It is clear that in such an arrangement chemical bonding can hardly take place. Actually, it is well-known that interlayer cohesion forces are of the van der Waals type. This fact is reflected by our H−F SCF energy (Table 1) which fails to describe any attractive interaction between layers. As a matter of fact, correlation is indispensable to account for this type of interactions. Our corrections for correlation, though approximate, indicate an energy stabilization of 8−12 kcal·mol^{-1} per unit cell. The (010) surface energy computed using these corrections is 0.19−0.31 J/m^2, while H−F SCF calculations yielded a repulsive energy value (−0.05 J/m^2).

The population analysis of Table 1 shows that there is no important modification of the electronic structure apart from some further polarization of Mo(1)−O(2) bonds. Looking at the DOS curve (Figure 2f), we see that the only difference with respect to the layer model is an accumulation of levels at the topmost part of the valence band, explained by the destabilization of some O(2) levels. We must note here that the absolute position of levels in bulk is arbitrary, contrary to the 1D or 2D models cases where the zero of potential is unambiguously defined at an infinite distance. The shift of bulk levels with respect to layer is, hence, meaningless. The valence bandwidth remains, practically, the same as in the case of the layer model.

From Table 1, we can see that the overall process of α-MoO_3 bulk formation from molecular MoO_3, as computed at the H−F SCF level, is exothermic by 83.5 kcal·mol^{-1}, while inclusion of correlation corrections yields a number of ∼105 kcal·mol^{-1}.

Concluding this section, it is interesting to compare the structure of MoO_3 with the structures of the other group 6A element trioxides. The CrO_3 solid may be regarded as built up of CrO_4 tetrahedra linked together to form chains with only weak van der Waals forces operating between them.[37] On the other hand, the WO_3 structure is a distorted variant of the "ReO_3" form, consisting of WO_6 octahedra linked by common O vertices.[37,38] In MoO_3, Mo atoms are, essentially, tetrahedrally coordinated with two additional electrostatic Mo−O bonds manifesting a tendency toward octahedral coordination. We can, therefore, state that there is an increasing tendency, going from WO_3 to CrO_3, to deviate from octahedral coordination, MoO_3

occupying an intermediate position. It was intriguing, at this point, to study an octahedral ReO_3-like structure for molybdenum trioxide. Such a structure was observed experimentally by Ganapathi et al.[38] and was found to be metastable, transforming to the stable layered MoO_3 structure. Thus, we carried out calculations adopting a regular "ReO_3" structure for MoO_3 bulk (space group *Pm*3*m*-*Oh*). At the H-F SCF level, we found that this form is less stable than the layered form of α-MoO_3 studied above, by 27 kcal·mol^{-1} (19 kcal·mol^{-1}, including corrections for correlation). In this model all Mo−O bonds are equivalent, with an optimal H−F SCF bond length value of 1.87 Å. All oxygen atoms have a net Mulliken charge −1.0, while Mo−O overlap population is 0.05, indicating a prevailing isotropic ionic character for this form of MoO_3.

4. The Adsorption of H_2O and CO Molecules on the (100) Surface of MoO_3.

A section of MoO_3 crystal parallel to the (100) plane results, as can be seen from Figure 1f, in a surface consisting of parallel ribbon structures (3.III) forming short-range steps due to the relative layer displacement. The formation of such a (100) surface implies the breaking of Mo(6)···O(3) type (Figure 1d) interactions. The corresponding surface energy was estimated to be ∼0.7 J/m^2, on the basis of H−F SCF calculations, whereas corrections for correlation yielded a value of 0.9 J/m^2. As a result of this Mo···O dissociation, the (100) surface contains molybdenum atoms with a coordination vacancy, acting like Lewis acids and capable of causing the adsorption of several molecules possessing a Lewis basic character. The importance of such acidic sites in catalytic processes has already been pointed out by many workers.[7,10] In what follows here, we examine the behavior of these Mo acidic sites by studying the adsorption of small molecules such as H_2O and CO.

The model used to simulate the (100) surface of MoO_3 was the double-ribbon model presented in section 3.IV. The analysis of Table 1 shows that the electronic structure of this model is quite similar to the corresponding structures of the layer and bulk models, and consequently, the use of a third ribbon accounting for bulk effects would not modify significantly the surface description while serious computational problems would be brought about.

4.I. Adsorption of H_2O Molecule. For the hydrated (100) surface we considered a 1:1 coverage on both sides of the double-ribbon model, which means that there is one water molecule per each surface Mo(1) vacant site.

The geometry optimization for the adsorption was done using a grid of points around equilibrium and yielded a Mo···O_w(water) distance of 2.350 Å and an angle $\angle O_wMo(1)O(5) = 82°$ (see Figures 1 and 5) at the H−F SCF level. The adsorption process was found to be exothermic by 21.5 kcal·mol^{-1} (∼32 kcal·mol^{-1}, with correlation corrections) with respect to the bare double-ribbon model plus isolated H_2O molecule. The repulsive interaction between adsorbed H_2O molecules, as estimated by considering isolated water monolayers with the same geometry as for the adsorbed layers, is 3.3 kcal·mol^{-1} (3.1 kcal·mol^{-1} with correlation corrections). The basis set superposition error (BSSE) was found, by a counterpoise calculation, to be small: 0.9 kcal·mol^{-1} of adsorbed H_2O.

In Figure 5 (bottom) we have reported the total and some projected DOS curves, the COOP (crystal orbital overlap population) curve for the Mo···O_w interaction, and the DOS curve of the isolated H_2O monolayer. We observe that all levels of the water monolayer are uniformly stabilized by interacting with the surface. The two highest occupied, nonbonding (H_2O lone pairs) levels have split up and spread over the lowest part of the valence band. However, the overlap population of the

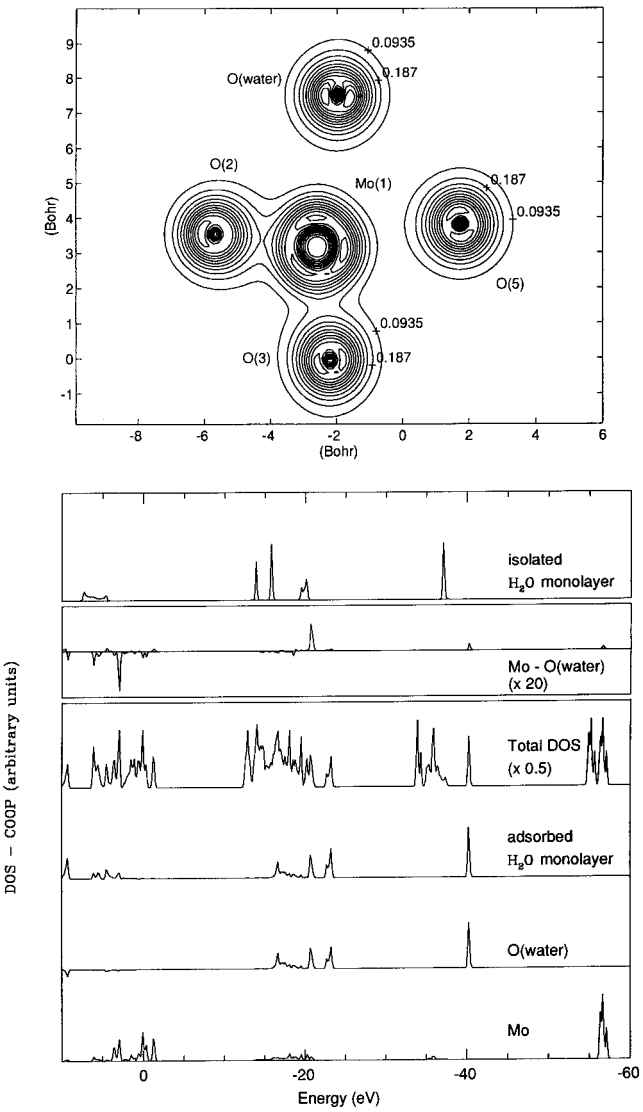

Figure 5. Bottom: Projected DOS curves for the hydrated double-ribbon model, COOP curve of the Mo(1)−O_w(water) interaction and DOS curve of the isolated H_2O monolayer. Top: Total electron density map of the hydrated double ribbon model, through a plane containing Mo(1), O(2, 3), and O_w atoms and perpendicular to the plane defined by the H_2O molecule.

Mo···O_w interaction is small (Table 2). Notice that the Mo−O_w COOP curve of Figure 5 has been magnified 20 times with respect to the projected DOS curves. Summing up to the Fermi level, we obtain an overlap population of 0.05, which is quite similar to the Mo(1)−O(5) value (Table 2).

The net Mulliken charges of Table 2 reveal a small electron transfer of 0.06 from H_2O to the surface, while polarization of water molecules increases slightly. The charge transferred to the surface is localized on oxygen atoms as Mo becomes more positive and the surrounding oxygen atoms increase their negative charges tending to the corresponding values of the bulk (Table 2). As a matter of fact, the adsorbed water molecules restore the 6-fold coordination of Mo atoms establishing around them a bulk-like environment.

Optimization of the interribbon distance of the hydrated model gave a value of 4.079 Å which is intermediate between the optimized values for the bare double-ribbon and layer models (4.222 and 3.920 Å, respectively).

The electron density map of Figure 5 (top) shows that the electronic distribution around oxygen atoms of adsorbed H_2O is very similar to that of O(5) atoms. This observation suggests a useful cluster model where interchain interactions are simu-

TABLE 2: Adsorption Energies Δ*E* (kcal·mol^{-1}), Adsorption Geometries,[a] Mulliken Net Charges *q*, and Overlap Populations *S* for the Adsorption of H_2O and CO Molecules on the (100) Surface of α-MoO_3

	H_2O adsorption			CO adsorption	
	noninteracting	adsorbed H_2O		noninteracting	adsorbed CO
ΔE^{SCF} [b]	0.0	21.4	ΔE^{SCF} [b]	0.0	9.2
d_{O_w-Mo} (Å)		2.350	d_{C-Mo} (Å)		2.701
∠O_wMoO(5), deg		82	d_{C-O} (Å)	1.129	1.120
ΔE^{cor} [c]	0.0	31.3	ΔE^{cor} [c]	0.0	15.7
$q[O_w]$	−1.01	−1.06	$q[C_{CO}]$	−0.01	−0.04
$q[H_w]$	+0.51	+0.56	$q[O_{CO}]$	+0.01	+0.09
q[Mo(1)]	+2.98	+3.05	q[Mo(1)]	+2.98	+3.00
q[O(2)]	−0.73	−0.78	q[O(2)]	−0.73	−0.75
q[O(3)]	−0.96	−1.02	q[O(3)]	−0.96	−0.99
q[O(4)]	−1.30	−1.31	q[O(4)]	−1.30	−1.31
$S[Mo(1)-O_w]$		0.05	$S[Mo(1)-C_{CO}]$		0.06
S[Mo(1)−O(2)]	0.25	0.22	S[Mo(1)−O(2)]	0.25	0.23
S[Mo(1)−O(3)]	0.05	0.11	S[Mo(1)−O(3)]	0.05	0.11
S[Mo(1)−O(4)]	0.07	0.06	S[Mo(1)−O(4)]	0.07	0.06
S[Mo(1)−O(5)]	0.07	0.06	S[Mo(1)−O(5)]	0.07	0.06
S[Mo(6)−O(3)]	0.07	0.06	S[Mo(6)−O(3)]	0.07	0.06
$S[O_w-H_w]$	0.25	0.24	S[C−O]	0.70	0.67

[a] The surface atom numbering is same as in Figure 1. [b] Absolute energy values of H_2O, $-16.89376E_h$, and of CO, $-21.23524E_h$. [c] Corrected for correlation using the Perdew 91 functional (ref 27); absolute energy values of H_2O, $-17.19000E_h$, and of CO, $-21.61048E_h$.

lated by H_2O molecules. However, care must be taken in such a model to describe properly the polarization effects induced by the bulk.

In order to investigate the influence of the interribbon polarization, we carried out calculations using a single-ribbon model of the (100) surface. The corresponding adsorption energy was found to be ∼13 kcal·mol^{-1} which is ∼8 kcal·mol^{-1} less than the value obtained with the double ribbon model.

4.II. Adsorption of CO Molecule. We considered, here again, a 1:1 coverage on both sides of the double-ribbon model. The CO molecules were chosen to interact with Mo atoms via the C atom, although it is not excluded that adsorption might occur via the O atom, as well. Considering a perpendicular approach (∠CMo(1)O(5) = 90°), we optimized the Mo−C and C−O bond distances. At the H−F SCF level we found an attractive interaction with an equilibrium Mo−C distance 2.701 Å while the C═O bond was slightly shortened (1.120 Å) with respect to the optimized H−F SCF value (1.129 Å) for the isolated CO molecule. The stabilization of the system was found to be 9.2 kcal·mol^{-1} of adsorbed carbon monoxide (∼16 kcal·mol^{-1} with correlation corrections). The repulsive interactions between adsorbed CO molecules were estimated to be small (∼0.3 kcal·mol^{-1}) and the BSSE is rather negligible (∼0.4 kcal·mol^{-1}).

As we can see from the DOS/COOP curves of Figure 6 (bottom), the mode of interaction is rather similar with the H_2O adsorption case. The two highest occupied levels of CO, representing a σ (electron pair on C) and a π orbital, have been split by the interaction with Mo but the overlap population brought about is small (Table 2). The remaining two levels of CO (O σ-pair and π-bond), shown in Figure 6, are not affected apart from a weak uniform downshifting.

As Table 2 shows, the adsorbed CO molecule exhibits some polarization. A small electron charge transfer toward the surface has, also, taken place. As we know, the isolated CO molecule possesses a weak dipole moment (∼0.12 D), with the negative pole being on the C end, due to a partial transfer of oxygen's p electron pair toward C to form a π bond. This effect seems to be reinforced by the interaction with the surface Mo atoms and the C═O bond is strengthened, which explains the small shortening of the C−O distance.

The charges and overlap populations of the surface atoms tend to mimic the MoO_3 bulk, but this effect is somewhat less pronounced than in the water adsorption case. Figure 6 (top) provides a picture of the electronic charge distribution around the adsorption site.

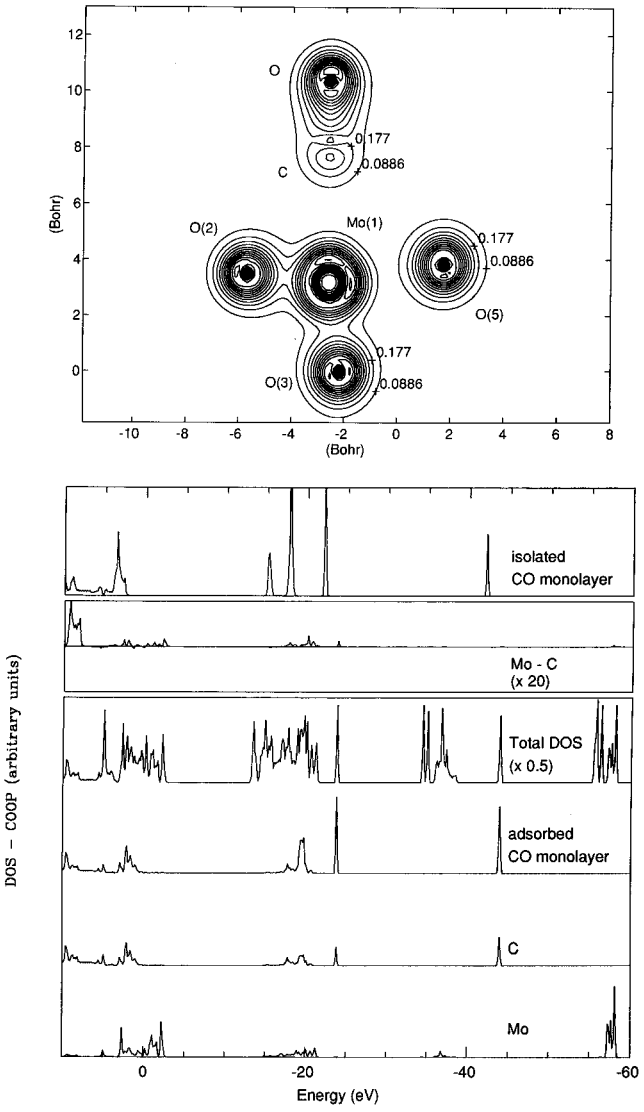

Figure 6. Bottom: Projected DOS curves for the double-ribbon + CO system, COOP curve of the Mo(1)−C interaction and DOS curve of the isolated CO monolayer. Top: Total electron density map of the double-ribbon + CO system, through a plane containing Mo(1), O(2, 3), and CO.

Replacing the double ribbon by a single ribbon model, we calculated, at the H−F SCF level, an adsorption energy of 6.5 kcal·mol^{-1}, while the equilibrium Mo−C distance was 2.790 Å. This means that, like in the case of water adsorption, bulk-induced polarization of the surface must be taken into account for a good description of the adsorption phenomenon.

In conclusion, we can say that the interaction of CO with Mo sites on the (100) surface of MoO_3 is essentially electrostatic since no significantt charge redistribution takes place between the adsorbent and the surface. This interaction is similar to the interaction of H_2O molecules, though weaker because of the lower dipole moment value of CO.

5. Concluding Remarks

1. Our periodic Hartree−Fock SCF results suggest that polymeric $(MoO_3)_x$ chains (Figure 1b) can be considered as the basic structural units of α-MoO_3 solid. More than a simple structural concept, these chains were found to preserve their chemical identity within α-MoO_3. They are held together by electrostatic interchain forces and are combined so as to form the natural layers of the solid. The energy gain upon forming a layer, as computed at the H−F SCF level, is 30 kcal per mole of MoO_3 formula unit (∼50 kcal·mol^{-1} including corrections for correlation), with respect to the isolated infinite chain model.

2. Concerning the three different types of Mo−O distances present in α-MoO_3 crystals, the following statements can be put forward: (i) The shortest (1.671 and 1.735 Å) Mo−O distances correspond to bonds reminiscent of Mo═O bonds in the MoO_3 molecule; the bonding occurs via two-electron coupling interactions (σ and π) and results in a notable electron transfer to oxygen atoms. (ii) The two intermediate (1.948 Å) Mo−O distances represent single bonds linking MoO_4 tetrahedra within $(MoO_3)_x$ chains. They are markedly ionic bonds with O atoms bearing a net Mulliken charge −1.31 (Table 1). (iii) The long (2.332 and 2.250 Å) Mo−O distances stem from the relative chain arrangement in the crystal, and represent interchain interactions of, essentially, electrostatic character.

3. The layered structure of α-MoO_3 is due to the significant deviation of Mo atoms from octahedral coordination, forming Mo═O bonds with partial covalent character. This feature is more pronounced in CrO_3 whereas in WO_3 the octahedral ReO_3-like structure prevails. We can, therefore, state that the tendency for octahedral coordination in MeO_3 (Me = Cr, Mo, W) crystal structures increases going down from Cr to W.

4. Formation of the (100) surface of α-MoO_3 involves breaking of interchain interactions. As a result, Lewis acidic (Mo atoms) and Lewis basic (O atoms) centers are present on this surface. The study of the adsorption of H_2O and CO molecules on such acidic Mo sites showed that interactions are, essentially, electrostatic and tend to restore the environment of Mo atoms in the bulk. Softer Lewis bases could lead to more reactive interactions involving charge transfer to the surface.

5. Useful cluster models could be used for the study of catalytic reactions on MoO_3 surfaces provided that (i) the polarization of the system is properly described and (ii) high-quality calculations including correlation are used to study reaction steps involving breaking of Mo−O bonds.

Acknowledgment. One of us (A.P.) wishes to thank the Région de Rhône-Alpes for a grant for a stay in Lyon, France.

References and Notes

(1) Greenwood, N. N.; EarnShaw, A. *Chemistry of the Elements*; Pergamon Press: New York, 1985.

(2) Magneli, A. *Acta Crystallogr*. **1953**, *6*, 495.

(3) Kihlborg, L. *Arkiv Kemi* **1963**, *21* (44), 471.

(4) Kihlbolg, L. *Arkiv Kemi* **1963**, *21* (34), 357.

(5) Bursill, L. A. *Proc. R. Soc. (London)* **1969**, *A311*, 267.

(6) Bertrand, O.; Floquet, N.; Jaquot, D. *Surf. Sci*. **1985**, *164*, 305.

(7) See, for example: Volta, J. C.; Portefaix, J. L. *Appl. Catal*. **1985**, *18*, 1 and references therein.

(8) Vedrine, J. C.; Coudurier, G.; Forissier, M.; Volta, J. C. *Catal. Today* **1987**, *1*, 261.

(9) Volta, J. C.; Tatibouet, J. M. *J. Catal*. **1985**, *93*, 467.

(10) Brückman, K.; Garbowski, R.; Haber, J.; Mazurkiewics, A.; Sloczynski, J.; Wiltowski, T. *J. Catal*. **1987**, *104*, 71.

(11) Tatibouet, J. M.; Germain, J. E. *J. Catal*. **1981**, *72*, 375.

(12) Tatibouet, J. M.; Germain, J. E.; Volta, J. C. *J. Catal*. **1983**, *82*, 240.

(13) Baiker, A.; Gasser, D. *Z. Phys. Chem*. **1986**, *149*, 119.

(14) Ziolkowski, J. *J. Catal*. **1983**, *80*, 263. Ziolkowski, J. *J. Catal*. **1983**, *84*, 317. Haber, J. *Structure and Reactivity of Surfaces*; Elsevier Science Publishers: Amsterdam, 1989. Zhou, B.; Chuang, K. T.; Guo, X. *J. Chem. Soc., Faraday Trans*. **1991**, *87* (22), 3695.

(15) Guerrero-Ruiz, A.; Abon, M.; Massardier, J.; Volta, J. C. *J. Chem. Soc., Chem. Commun*. **1987**, 1031.

(16) Guerrero-Ruiz, A.; Blanco, J. M.; Aguilar, M.; Rodriguez-Ramos, I.; Fierro, J. L. G. *J. Catal*. **1992**, *137*, 429.

(17) Smith, M. R.; Ozkan, U. S. *J. Catal*. **1993**, *141*, 124; **1993**, *142*, 226.

(18) Mestl, G.; Ruiz, P.; Delmon, B.; Knözinger, H. *J. Phys. Chem*. **1994**, *98*, 11269.

(19) Firment, L. E.; Ferretti, A. *Surf. Sci*. **1983**, *129*, 155.

(20) Broclawik, E.; Foti, A. E.; Smith, V. H., Jr. *J. Catal*. **1978**, *51*, 380; **1981**, *67*, 103.

(21) Sylvestre, J. *J. Am. Chem. Soc*. **1987**, *109*, 594.

(22) Mehandru, S. P.; Anderson, A. B.; Brazdil, J. F.; Grasselli, R. K. *J. Phys. Chem*. **1987**, *91*, 2930. Anderson, A. B.; Edwin, D. W.; Kim, Y.; Grasselli, R. K.; Burrington, J. D.; Brazdil, J. F. *J. Catal*. **1985**, *93*, 222.

(23) Kang, D. B.; Lee, E. S. *Bull. Korean Chem. Soc*. **1987**, *8* (6), 482.

(24) Rappé, A. K.; Goddard, W. A. III. *J. Am. Chem. Soc*. **1980**, *102*, 5115; *Nature* **1980**, *285*, 311; *J. Am. Chem. Soc*. **1982**, *104*, 3287; *J. Am. Chem. Soc*. **1982**, *104*, 448.

(25) Rahmouni, A.; Barbier, C. *J. Mol. Struct. (THEOCHEM)* **1995**, *330*, 359.

(26) Pisani, C.; Dovesi, R.; Roetti, C. *Hartree-Fock ab initio Treatement of Crystalline Systems, Lecture Notes in Chemistry*; Springer-Verlag: Heidelberg, 1988; Vol. 48.

(27) Perdew, J. P. In *Electronic Structure of Solids*; Ziesche, P., Eschwig, H., Eds.; Academic Verlag: Berlin, 1991.

(28) Dovesi, R.; Roetti, C.; Freyria-Fava, C.; Apra, E.; Saunders, V. R.; Harrison, N. M. *Phil. Trans. R. Soc. London A* **1992**, *341*, 203.

(29) Colle, R.; Salvetti, O. *Theor. Chim. Acta* **1975**, *37*, 329.

(30) Hay, P. J.; Wadt, W. R. *J. Chem. Phys*. **1985**, *82*, 299.

(31) Bouteiller, Y.; Mijoule, C.; Nizam, M.; Barthelat, J. C.; Daudey, J. P.; Pelissier, M.; Silvi, B. *Mol. Phys*. **1988**, *65* (2), 295.

(32) Unpublished results of the same authors as in ref 31.

(33) Dovesi, R.; Saunders, V. R.; Roetti, C. CRYSTAL92 User Manual, University of Turin (Italy), SERC Daresbury Laboratory (U.K.). Dovesi, R.; Pisani, C.; Roetti, C. and Saunders, V. R. CRYSTAL88 in QCPE, Department of Chemistry, Indiana University, Bloomington, IN, 1988.

(34) Frisch, M. J.; Trucks, G. W.; Schlegel, H. B.; Gill, P. M. W.; Johnson, B. G.; Robb, M. A.; Cheeseman, J. R.; Keith, T. A.; Petersson, G. A.; Montgomery, J. A.; Raghavachari, K.; Al-Laham, M. A.; Zakrewski, V. G.; Ortiz, J. V.; Foresman, J. B.; Cioslowski, J.; Stefanov, B. B.; Nanayakkara, A.; Challacombe, M.; Peng, C. Y.; Ayala, P. Y.; Chen, W.; Wong, M. W.; Andres, J. L.; Replogle, E. S.; Gomperts, R.; Martin, R. L.; Fox, D. J.; Binkley, J. S.; Defrees, D. J.; Baker, J.; Stewart, J. P.; Head-Gordon, M.; Gonzalez, C.; Pople, J. A. *Gaussian 94*; Gaussian, Inc.: Pittsburgh, PA, 1995.

(35) DeMaria, G.; Burns, R. P.; Drowart, J.; Inghram, M. G. *J. Chem. Phys*. **1960**, *32*, 1373.

(36) Berkowitz, J.; Inghram, M. G.; Chupka, W. A. *J. Chem. Phys*. **1957**, *26*, 842.

(37) Wyckoff, R. W. G. *Crystal Structures, Vol. 2 Inorganic Compounds*; Interscience Publishers: New York, 1964.

(38) Ganapathi, L.; Ramanan, A.; Gopalakrishnan, J.; Rao, C. N. R. *J. Chem. Soc., Chem. Commun*. **1986**, 62.

JP953727W